



OPEN Microphysiological system with integrated sensors to study the effect of pulsed electric field

Neringa Bakute^{1✉}, Eivydas Andriukonis¹, Kamile Kasperaviciute¹, Jorunas Dobilas², Martynas Sapurov², Gatis Mozolevskis³ & Arunas Stirke^{1,3✉}

This study focuses on the use of pulsed electric fields (PEF) in microfluidics for controlled cell studies. The commonly used material for soft lithography, polydimethylsiloxane (PDMS), does not fully ensure the necessary chemical and mechanical resistance in these systems. Integration of specific analytical measurement setups into microphysiological systems (MPS) are also challenging. We present an off-stoichiometry thiol-ene (OSTE)-based microchip, containing integrated electrodes for PEF and transepithelial electrical resistance (TEER) measurement and the equipment to monitor pH and oxygen concentration in situ. The effectiveness of the MPS was empirically demonstrated through PEF treatment of the C6 cells. The effects of PEF treatment on cell viability and permeability to the fluorescent dye Dapi were tested in two modes: stop flow and continuous flow. The maximum permeability was achieved at 1.8 kV/cm with 16 pulses in stop flow mode and 64 pulses per cell in continuous flow mode, without compromising cell viability. Two integrated sensors detected changes in oxygen concentration before and after the PEF treatment, and the pH shifted towards alkalinity following PEF treatment. Therefore, our proof-of-concept technology serves as an MPS for PEF treatment of mammalian cells, enabling in situ physiological monitoring.

Keywords Microphysiological system, Microfluidics, Pulsed electric field, Sensors, PDMS, OSTE

Electroporation is a technique that modifies the permeability of a cell membrane by subjecting it to a pulsed electric field (PEF). PEF causes changes in the cell's bilipid membrane, creating hydrophilic pores through which molecules can move in and out of a cell¹. The effects of PEF treatment on a cell depend on various factors, including the intensity, duration, number of pulses, and frequency of the applied electric field. Reversible electroporation is a process that introduces temporary changes to membrane structure to enable gene electrotransfer, drug delivery or tissue engineering while preserving the integrity of the cells. This technique offers a safe and effective means of achieving these objectives without harming the cell². Conversely, if the impact of the electric field is too severe and the membrane undergoes transient rearrangements, irreversible electroporation occurs, leading to cell death. The latter process is widely applied in medicine³ and the food industry⁴.

The conventional approach to PEF treatment typically involves batch electroporation of statically cultured cells. However, culturing cells within a flow system provides a more accurate representation of an organism's cells. Such systems create flow-induced shear stresses, facilitate cell-to-cell or tissue-to-tissue interactions, and maintain low media-to-cell and cell-to-tissue volume ratios. The flow systems allow for automated and continuous media changes to support nutrient replenishment. Furthermore, it enables the extraction and division of supernatants for further analysis⁵. While the field has predominantly concentrated on developing microphysiological systems (MPS) models, there is a growing acknowledgement that integrating biosensing capabilities would enable real-time monitoring of the condition and function of cells, tissues or organs⁶. Traditional analytical methods are not well-suited for miniaturized MPS platforms due to their reliance on manual sample collection from the microfluidic system, large working volumes, and frequent disruptions to the system⁷. Instead, there is a strong desire for an integrated system that seamlessly combines organ models, microfluidic units and biosensors. Ideally, this system would operate continuously and fully automated for extended periods, meeting the needs of researchers and allowing for enhanced functionality. As an illustration, numerous MPS have been developed to

¹Laboratory of Bioelectrics, State Research Institute, Center for Physical Sciences and Technology, Sauletekio Ave. 3, 10257 Vilnius, Lithuania. ²Nanostructured Materials and Sensors Laboratory, State Research Institute, Center for Physical Sciences and Technology, Sauletekio Ave. 3, 10257 Vilnius, Lithuania. ³Micro and Nanodevices Laboratory, Institute of Solid State Physics, University of Latvia, Kengaraga Str. 8, Riga 1063, Latvia. ✉email: neringa.bakute@ftmc.lt; arunas.stirke@ftmc.lt

measure real-time parameters like glucose and lactate levels, oxygen levels, ions, extracellular acidification rate, and protein biomarkers within systems^{8–10}. Moreover, transepithelial electrical resistance (TEER) is utilized to study the barrier function, as demonstrated that PEF non-invasively induces disruption to the blood–brain barrier (BBB)^{10–13}. A recent publication has showcased MPS with integrated real-time TEER measurement, which can facilitate *ex vivo* mouse colon tissue observation for a duration of up to three days¹⁴. We recently introduced the application of PEF for the induction of the nuclear factor κ B (NF- κ B) pathway-controlled transcription system, which encodes a secreted embryonic alkaline phosphatase protein (SEAP) protein under the control of PEF inducible promoter carrying NF- κ B recognition sites¹⁵. To investigate the application of PEF on cells or cellular structures, there is a need to develop a suitable MPS capable of accommodating such treatment.

The main materials for the fabrication of microchips are silicon, paper, glass, and polymers^{16,17}. Polydimethylsiloxane (PDMS) is a versatile silicone polymer used in many microchips. PDMS offers ease of fabrication, optical transparency, gas permeability, and biocompatibility, making it suitable for long-term cell culture, cell screening, and biochemical studies¹⁸. PDMS also enables direct integration of inlets and outlets, including valves and pumps, directly into the microchip structure¹⁹. Furthermore, PDMS is relatively inexpensive compared to materials like silicon and glass. Despite its numerous advantages, PDMS has certain limitations. PDMS has a porous structure that can lead to the absorption of small molecules. This includes molecules from cell culture media and test substances. Organic solvents can be absorbed by PDMS, causing deformation in microchannels²⁰. Chips with PDMS may experience the leaching of uncrosslinked oligomers. Cured PDMS often contain residual polymer chains that have not fully crosslinked. These uncrosslinked oligomers can freely diffuse within the PDMS material and may leach when in contact with a solution^{21,22}. Moreover, high flow rates within the PDMS microchannels can lead to the expansion of the microchannels²³. As a result, PDMS-based microfluidic chips may not be suitable for pharmaceutical testing^{22,24,25}.

To overcome the limitations of PDMS, the surface of the microchannel can be modified using non-stick and inert materials such as perfluorinated polymers (e.g., Teflon AF, Cytop), Parylene, and sol–gel-based silica nanoparticles^{22,26–29}. Another option is to replace PDMS with alternative polymers, such as off-stoichiometry thiol-ene (OSTE)^{30,31}. OSTE shows promise as an alternative to PDMS due to its significantly reduced absorption of small molecules, while still offering ease of fabrication and maintaining other essential characteristics for microfluidics, such as biocompatibility, and repeatability²⁸.

The current study details the development of an MPS device that enables PEF treatment of mammalian cells with simultaneous monitoring of extracellular microenvironment parameters such as oxygen level, pH and TEER. The microchip is fabricated using OSTE as a polymer-forming structure. The performance of MPS for PEF treatment of mammalian cells with PEF was confirmed using the rat glioma C6 cell line in stop flow and continuous flow electroporation. We demonstrated an excellent viability rate even at an electric field of up to 10 kV/cm. The permeability reached a maximum value at 1.8 kV/cm electric field strength with different pulse numbers in stop flow and continuous flow modes. The monitoring of physiological parameters revealed a decrease in oxygen concentration without PEF treatment, whereas with PEF treatment oxygen concentration showed an increase and pH shift to alkalinity. Lastly, the ability to measure TEER was demonstrated with the same electrodes, used for PEF.

Results

Microchip fabrication

The microchip was fabricated by soft lithography technique using a dual-curable polymer OSTE. A general microchip fabrication scheme is depicted in Fig. 1. Briefly, the fabrication required two molds: a 3D printed master mold was needed to cast a secondary PDMS mold. A cyclic olefin copolymer (CoC) slide with thermally deposited gold electrodes was placed in the PDMS mold and secured with a custom-made clamping bracket. OSTE was injected into the space between the PDMS and the CoC slide through an inlet tube and partially cured under UV light. This treatment was carried out on two analogous slides. The polycarbonate (PC) membrane was glued onto the adhesive OSTE surface of the bottom slide and fully heat-cured. The upper slide was prepared afterward. After the initial UV treatment, two oxygen spot sensors were glued onto the CoC in their dedicated pockets. Then the upper slide, which still contained a “sticky” OSTE surface, was glued on the bottom one, and the full microchip underwent final heat curing. Finally, mini-luer ports were glued to the inlet and outlet holes of the microchip channels. The microchip was then placed in a support jig, where the bottom and top parts contain electrical contacts for PEF processing and the top part contains optical sensors for oxygen and pH measurements.

The presented technology has at least two key aspects: (1) the microchip was fabricated by soft lithography allowing for easy modifications of channel geometry, electrode number, and positioning; (2) CoC, OSTE and PC membrane constrain the channel and not PDMS, which eliminates adverse properties of PDMS such as molecular absorption, gas permeation, and channel deformation.

Design of the microchip

A microfluidic chip was fabricated in the format of a microscopy slide. The PEF treatment chamber consists of four independent parallel plate pairs of 2 × 2 mm wide electrodes with 2 mm spacing between them (Fig. 2a). The electrodes are in direct contact with the fluid in the PEF treatment chamber. Any combination of the electrode pairs could be used together based on connection to the power source. Two 3 mm diameter oxygen sensor spots were integrated upstream and downstream of the PEF treatment chamber in the upper subchannel. The pH sensing area is situated further down the channel. The channel width is 2 mm at the electroporation area and 1 mm at the pH sensing area. Channel height ranges from 0.75 to 0.85 mm and is divided into two subchannels by a porous PC membrane (Fig. 2b), providing a surface for cell adhesion and growth.

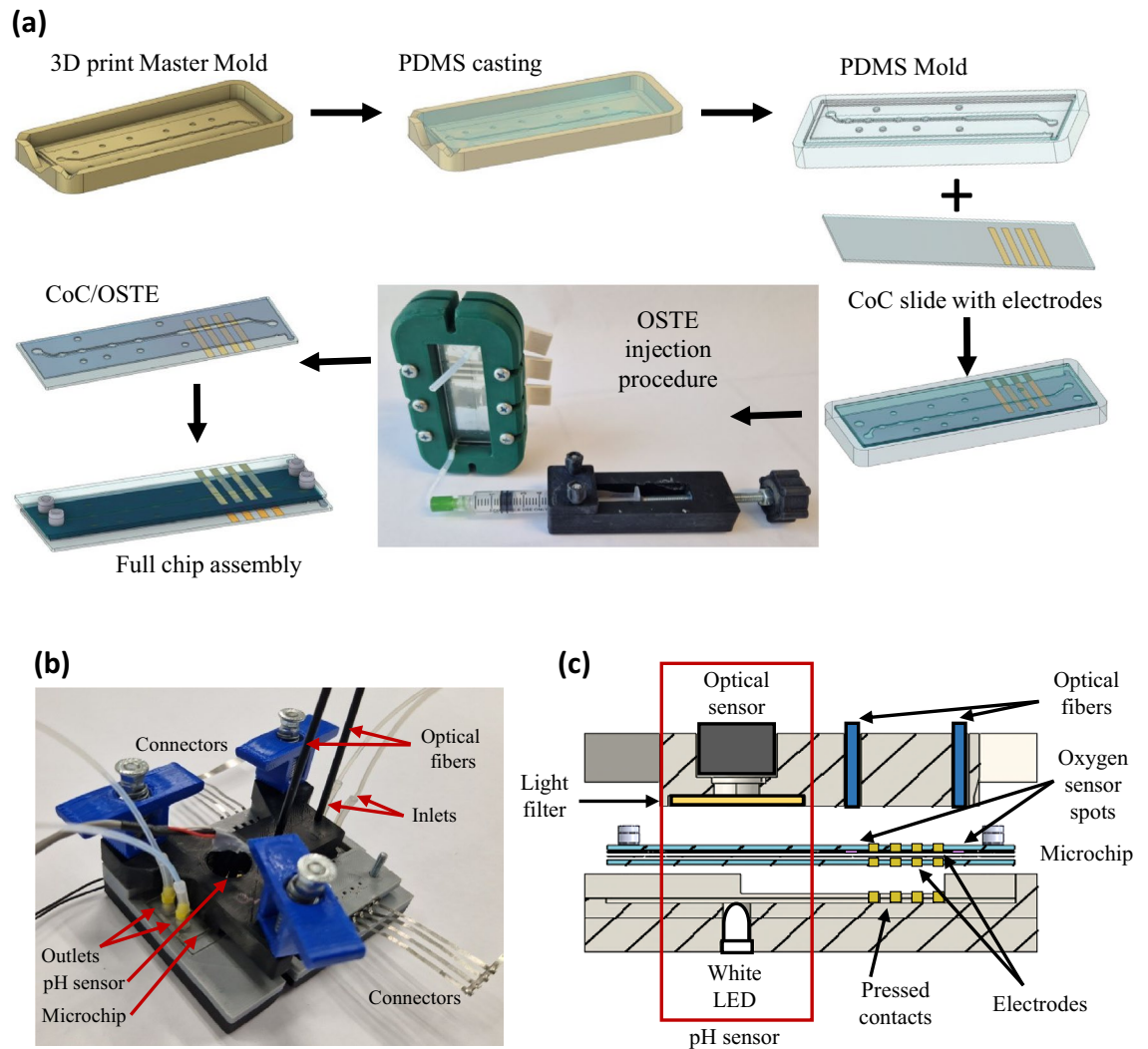


Figure 1. (a) Schematic microchip fabrication process. (b) MPS prototype. (c) Cross-section and decomposition of the supporting jig.

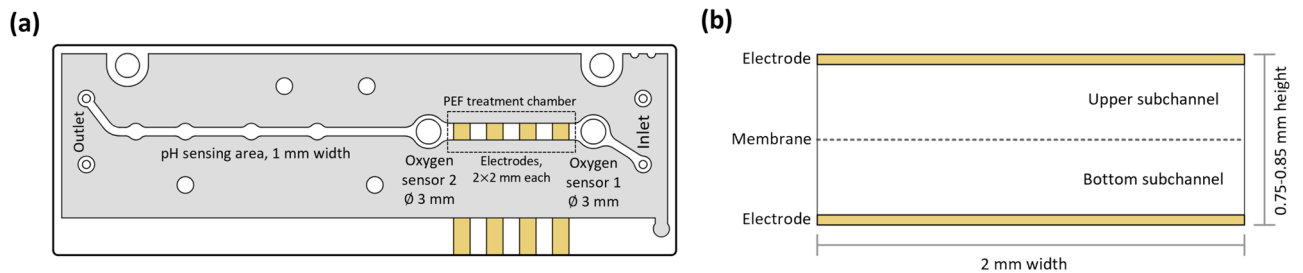


Figure 2. Schematic representation of the microchip. (a) The upper CoC/OSTE/O₂ slide and (b) cross-section of the channel at the electrodes in the PEF treatment chamber.

Simulation of the electric field in the microchip

A schematic representation of electric field distribution in the microchannel is presented in Fig. 3a. The electric field was generated only in the area between parallel plate electrodes. Meanwhile, the electric field was negligible in the gaps between the electrodes (Supplementary S1). COMSOL Multiphysics software package was used for the electric field simulation across two parallel plane electrodes (2 × 2 mm and 0.8 mm height) with a porous insulating membrane with different pore sizes and porosity: (1) 0.4 μm pores with 18.8% porosity and (2) 3 μm pores with 21.2% porosity. Both membranes are of similar thickness: (1) 25 μm and (2) 22 μm, respectively. For

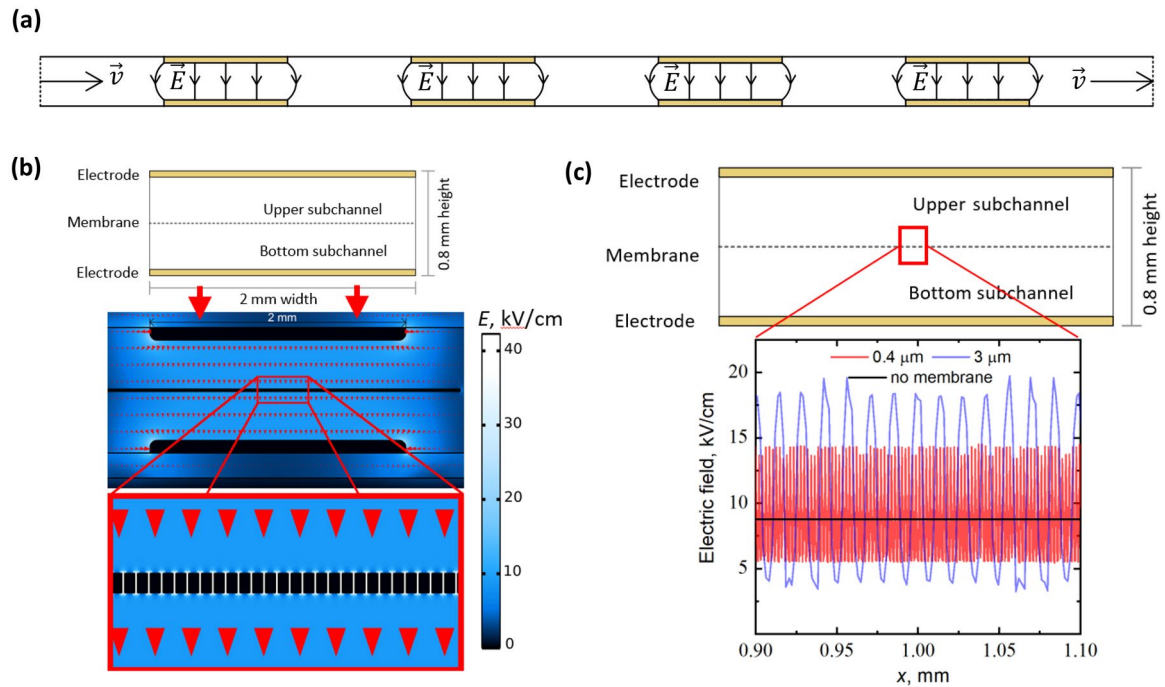


Figure 3. Electric field distribution in the microchip. (a) Schematic representation of electric field lines in the PEF treatment chamber. \vec{v} is fluid flow rate, \vec{E} —electric field vector. (b) Simulation results of electric field distribution in the microchip using COMSOL Multiphysics. The membrane with a pore size of $3\ \mu\text{m}$ and porosity of 21.2% was used; 800 V voltage potential is applied which is expected to produce a 10 kV/cm electric field in the channel without membrane. The colour gradient represents the electric field strength in kV/cm. Red triangles show the direction of the electric field. (c) Simulation results of the electric field strength distribution across the microchip without the membrane (black line) and $0.5\ \mu\text{m}$ above the membrane. Blue and red lines correspond to oscillations in the microchip with pores sizes of $3\ \mu\text{m}$ and $0.4\ \mu\text{m}$, respectively.

comparison, electric field distribution without the membrane was also calculated. 800 V potential difference was selected for the simulation to achieve up to 10 kV/cm electric field.

The electric field simulations showed a roughly uniform distribution of the electric field in the subchannels ($\sim 9\ \text{kV/cm}$) (Fig. 3b), with a minor decrease in comparison with a channel without membrane ($\sim 10\ \text{kV/cm}$). However, the electric field near the membrane was amplified by approximately a factor of 2. In addition, electric field strength oscillates in space, being at its maximum above the void space, thus the distribution of the field above the membrane depends on the membrane parameters (Fig. 3c). The membrane with a pore size of $3\ \mu\text{m}$ demonstrates a greater electric field distribution near the membrane and higher oscillation amplitude compared to the membrane with smaller pores ($0.4\ \mu\text{m}$). In contrast, the membrane with smaller pores exhibits a more uniformly distributed electric field and lower oscillation amplitude. As a result of these effects, the PEF treatment can be focused on the region near the membrane.

Cell viability and permeability after PEF treatment in the microchip

In the realm of PEF microchips, various electrode configurations have been employed to carry out electroporation. Electrodes are either inserted into the access reservoirs or integrated within the microchip^{32,33}. The integrated electrodes can have a one-plane geometry, parallel plates, or a 3D electrodes. The electrodes in our microchip are configured as parallel plates. The PEF treatment chamber consists of 4 identical independent pairs of electrodes and 3 gaps of the same dimensions between them (Figs. 2a, 3a). This means that when the cells are injected into the PEF treatment chamber, only 4/7 volumes of cells will experience the electric field. For the remaining cells to be electroporated, the cell suspension has to be pushed over the volume of one electrode, which demands manual handling. The volume was calculated using formula (1) (“Material and methods”). However, the experimental procedure could be greatly simplified by conducting the PEF treatment in continuous flow mode, whereby the flow and PEF treatment are performed simultaneously. In this mode, cells flow through the entire PEF treatment chamber, where the electrodes and gaps are located, resulting in the presence or absence of the electric field, respectively. Consequently, it is necessary to calculate the flow rate (using formula (2), as outlined in the “Material and methods” section) to determine the exact number of pulses that should be applied to the cells as they pass through the entire PEF treatment chamber. These specific numbers of pulses are referred to as pulses per cell.

To assess the efficacy of the PEF treatment in microchips, we have conducted studies using both flow modes: stop and continuous. A suspension of rat glioma cell line C6 was used for the electroporation studies in 0–10 kV/cm electric field range, 100 μs pulse duration, and 1 Hz repetition rate. The stop flow electroporation was performed with an electric field from 1.8 to 10 kV/cm (Fig. 4a). The results demonstrated no change in cell viability

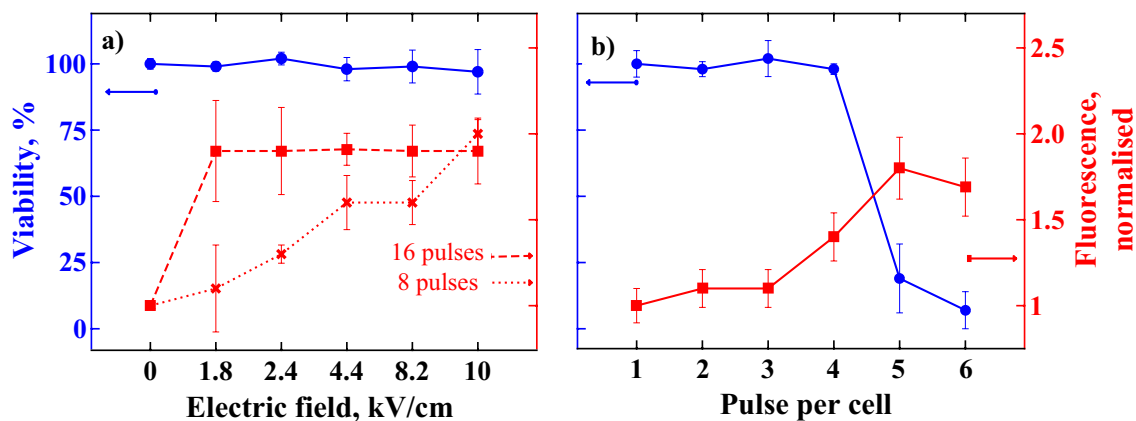


Figure 4. Effect of PEF treatment on C6 cell and permeability in (a) stop flow and (b) continuous flow electroporation. In (a) 0–10 kV/cm electric field range with either 8 or 16 pulses was used. In (b) electric field of 10 kV/cm was applied for viability experiments, and 1.8 kV/cm for permeability experiments with the range of 0–128 pulses per cell. In both (a) and (b) PEF treatment was performed with 100 μ s pulse duration and 1 Hz repetition rate. Permeability quantified as fluorescence normalised to the non-treated control; number of experiments $n \geq 3$; error bars represent standard deviation.

after PEF treatment with 8 pulses in all tested electric fields. The permeability after PEF treatment was studied with 8 and 16 pulses applied using a fluorescent intercalating dye DAPI. The permeability increased progressively with higher electric field strengths with 8 pulses. As evidenced by the fluorescence ratio compared to the non-PEF treated control. However, with 16 pulses at 1.8 kV/cm, cell permeability to DAPI reached the same level as with 8 pulses at 10 kV/cm. Hence, using 16 pulses at an electric field strength of 1.8 kV/cm was sufficient to achieve maximum permeability to DAPI.

In continuous flow mode, permeability increased slightly with 32 pulses per cell at 1.8 kV/cm reaching a maximum increase at 64 and 128 pulses. This increase was comparable to 1.8 kV/cm with 16 pulses condition observed in stop flow experiments. Additionally, exposure to continuous flow PEF treatment at the highest electric field strength of 10 kV/cm with 8–32 pulses per cell did not significantly affect cell viability compared to the control.

However, continuous flow electroporation with 64 and 128 pulses per cell significantly reduced cell viability by 80% and 93%, respectively (Fig. 4b).

Prediction of affected area in continuous PEF

According to the viability results 64 pulses are required to reduce the viability at 10 kV/cm in continuous flow. Meanwhile, no change in cell viability in stop flow electroporation with 8 pulses was observed. However, permeability studies showed that the maximum permeability was obtained at the electric field of 1.8 kV/cm with 16 pulses in stop flow mode, meanwhile, continuous flow requires 64 pulses at the same electric field. This means four times as many pulses in continuous flow electroporation should be provided to achieve equivalent permeability as in stop flow mode. These results can be explained with the following assumptions: (1) the electric field gradient affected only a certain area of the membrane; (2) in stop flow cells are in semi-stationary conditions, i.e., cells remain roughly stationary during the whole pulsation process and the energy was delivered to the same area of the membrane multiple times (successfully electroporated area, Fig. 5a). (3) In continuous flow PEF, cells undergo random rotation throughout the entire microchannel, including both the areas: between the parallel plate electrodes and the gaps. Figure 5b specifically focuses on the electrode regions, where two stages can be distinguished: the pulse period when the electric field interacts with the cells (the pulse period represents the exact moment of an electric field application), and the relaxation period during which no electric field is present. Cell rotation occurs during both periods. Due to these rotations, the affected area of a cell becomes larger, while the successfully electroporated area become smaller, in comparison with semi stationary conditions (Fig. 5a).

A theoretical model for the determination of the affected area of the membrane was created using MATLAB software. In continuous flow, a portion of the total area of the cell was affected by the electric field. Afterwards, the cell was allowed to randomly rotate by the angle θ and the cell was affected again in another spot. This is repeated N times until the affected area overlaps at least n times in one spot. Assuming cells remain approximately stationary in stop flow mode, the affected area overlaps, meaning n was the number of pulses required. The size of affected area was depending on the effective ratio N/n and is presented in Fig. 6. From our experimental results, the effective ratio of N/n was equal to 4, thus, the affected area was determined as 16% (intersection of red lines, Fig. 6), i.e. 16% of the cell membrane must receive pulses to get the same permeability level as in stop flow mode.

Oxygen measurement experiments

The microchip was equipped with two oxygen sensors—one upstream and one downstream of the PEF treatment chamber (Fig. 2a), both sensors are positioned equidistantly from the edge electrodes. When the flow is activated, Sensor 1 comes into contact with the fresh medium that passes through the electrodes, and Sensor 2 comes into contact with the medium after a potential PEF treatment. Therefore, Sensor 1 measures the oxygen

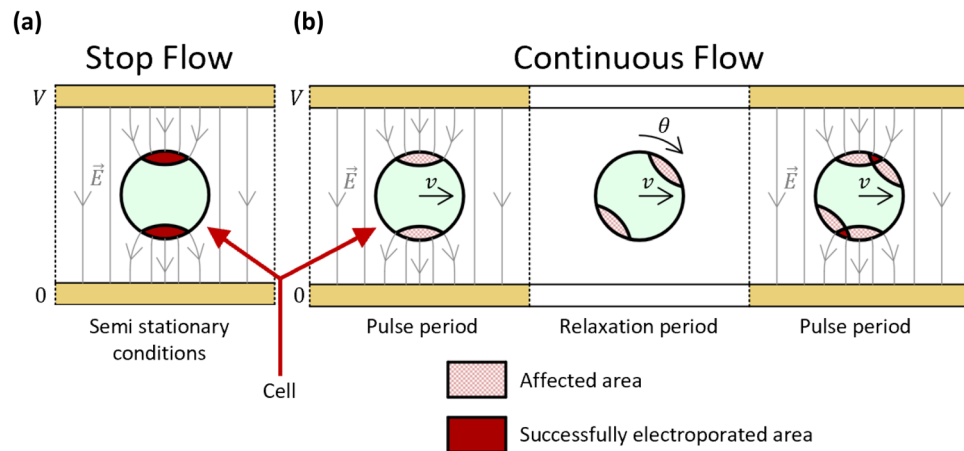


Figure 5. Schematic representation of how cells are affected in (a) stop flow and (b) continuous flow PEF. v stands for fluid flow rate, \vec{E} —electric field vector, θ —random angle of rotation V —applied voltage on the electrode, and 0 —ground voltage on the electrode.

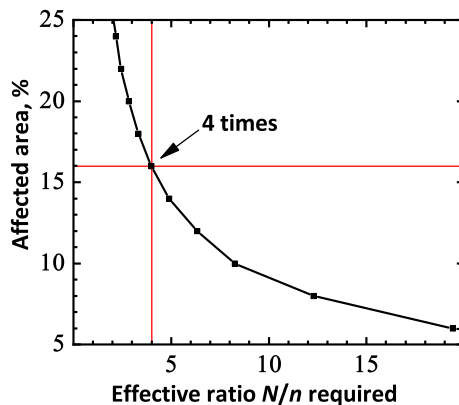


Figure 6. Surface area and pulse ratio relationship of continuous and stop flow electroporation modes as calculated in MATLAB software. N and n correspond to pulse number in continuous flow and stop flow modes, respectively; red lines mark the match with experimental data.

concentration prior to the PEF treatment, while Sensor 2 records the concentration after the treatment. Oxygen measurement experiments were conducted utilizing PEF as the stimulus to evaluate the effectiveness of MPS in capturing changes in oxygen concentration. Data on oxygen concentration were collected from both sensors prior to and immediately following the cessation of PEF.

In the absence of PEF treatment (0 kV/cm), there was a significant decrease in oxygen concentration by $0.14 \pm 0.07\%$ at sensor 2 compared to sensor 1 (Fig. 7a). This decrease was notable when compared to the control sample containing only buffer, which showed a smaller decrease of $0.01 \pm 0.07\%$. However, when cells were to PEF, a noticeable increase in oxygen concentration of 0.14%, 0.13%, 0.09%, and 0.03% was observed at electric fields of 1.8, 2.4, 4.4, and 8.0 kV/cm, respectively. Notably, the buffer samples at lower electric fields (1.8 and 2.4 kV/cm) exhibited distinct variations from the cell suspension, indicating that these variations were specifically caused by the effect of PEF on the cells. However, at 4.4 and 8.0 kV/cm, both the cells and buffer showed similar changes in oxygen concentration.

pH measurement

The optimal pH for mammalian cell culture media is around 7.2–7.4, with some cell lines preferring slightly lower or higher pH values. Drastic changes in pH affect cell viability; hence, the pH must be maintained within a range of 6.5–8.5. Bicarbonate is a commonly used buffering agent in culture media, the pH of which is highly dependent on the CO_2 content; while another buffering agent HEPES is not influenced by CO_2 . To monitor the pH in the media, a pH indicator phenol red is commonly used with a colour change from yellow at acidic pH to purple at alkaline pH. Due to cellular metabolic processes, the pH of the medium changes towards the acidic side; moreover, the PEF treatment has the potential to bring alterations in pH levels^{34,35}.

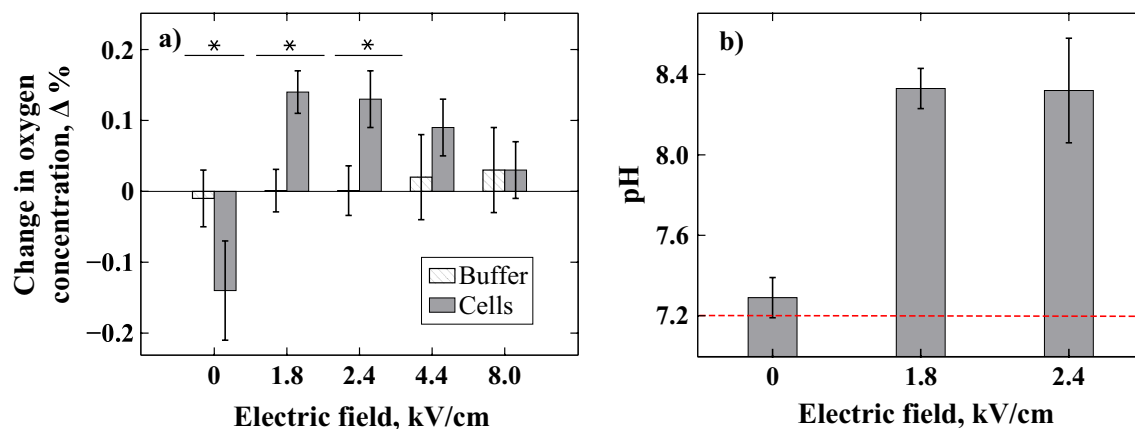


Figure 7. Effect of PEF treatment on (a) oxygen concentration difference between two sensors and (b) pH, immediately after PEF. PEF treatment was performed in the stop flow mode with various electric fields, 16 pulses, 100 μ s pulse duration, and 1 Hz repetition rate. Number of experiments $n \geq 3$; asterisks* correspond to statistically significant difference ($p \leq 0.00001$). The dashed line in (b) represents the buffer baseline. Error bars show standard deviation.

The principle of the optical pH meter, integrated into MPS (Fig. 1b), is based on the colour change of phenol red (Supplementary S2). To validate the pH-meter's performance, we evaluated pH changes following PEF treatment in C6 cells resuspended in media containing phenol red and bicarbonate and HEPES (Fig. 7b). Two buffering agents ensure stable pH levels despite the lower CO_2 content compared to the CO_2 incubator environment. PEF treatment was performed at either 1.8 kV/cm or 2.4 kV/cm electric field with 16 pulses, since these electric field parameters are optimal for permeability. The effect on pH of PEF-treated and non-treated control was tested. The initial pH of the media was 7.2. Cells without PEF had pH of 7.29 ± 0.06 . PEF treatment increased the pH to 8.3 ± 0.14 with 1.8 kV/cm and 8.3 ± 0.26 with 2.4 kV/cm (Fig. 8b).

TEER measurement

The experiments were performed with cells in suspension. The results of TEER measurement revealed a $60 \pm 4\%$ reduction of impedance after cell injection to the microchip compared to plain buffer. No significant change in TEER before and after PEF treatment was observed due to the lack of a confluent cell layer. We are confident that these discoveries, along with the chip design that utilizes the same electrodes for both PEF and TEER applications, have the potential to be implemented in future applications.

Discussion

PEF, as a physical method for electrotransfer or inactivation of the cells, is used both in the medical and food industries. Nowadays, the field of PEF research is moving towards the microfluidics scale to perform PEF experiments and monitor the effects of PEF on cells under more precise conditions in microfluidic systems. Real-time monitoring sensors and instruments integrated into MPS systems enable to collect the experimental data in situ. However, MPS development faces at least two challenges: firstly, standard instruments for monitoring physiological parameters are not suitable for microfluidic applications, so specific sensors have to be provided for in situ monitoring of microfluidic systems. The second challenge relates to PDMS, a polymer used in soft lithography for microchip fabrication. Despite the advantages of PDMS, it has some undesirable properties as the absorption of small molecules, channel expansion and release of unbound crosslinkers into the inner channel, which leads to a distortion of the experimental results and the inability to adapt such systems to pharmaceutical applications.

In the study, we employed OSTE-based microchip fabrication³¹ to develop MPS with incorporated electrodes for PEF treatment. The electrodes can be used for both PEF treatment and TEER measurement. Moreover, the MPS has integrated oxygen and pH sensors for microphysiological monitoring.

Simulations of the electric field distribution in the microchannel with and without membranes were performed. The porous insulating membrane in the middle of the channel does not substantially alter the electric field in the subchannel (9 kV/cm with vs. 10 kV/cm without membrane). In contrast, at the very surface of the membrane—a few microns above it—the electric field strength was approximately doubled. In our experiment, the PEF treatments were performed with suspension cells that were distributed over the entire height of a single subchannel. Therefore, the effect of electric field enhancement on the PEF results in suspension cells was negligible when compared to the 0.4 mm height of the subchannel. However, it is important to consider the enhancement if the experiments were performed using cells that are in close proximity to the PC membrane, such as in the case of adherent cells cultured directly on the membrane surface.

Our microchip utilizes parallel plate electrodes that replicate the structure found in conventional electroporation systems available in the market. To test the efficiency of the microchip as an electroporation cuvette, PEF treatment of mammalian cells in suspension was executed. The cell viability was tested in stop flow experiments and revealed no change when 8 pulses of 0–10 kV/cm electric field were applied (Fig. 4a). In contrast, cell viability decreased in continuous flow electroporation with 64 and 128 pulses delivered at 10 kV/cm (Fig. 4b). The

permeability was evaluated using the impermeable fluorescent dye DAPI whose fluorescence correlates to the permeabilization of the cellular membrane. The results of stop flow electroporation revealed a gradual increase in permeability with the increasing electric field up to 10 kV/cm with 8 pulses (Fig. 4a). To provide an electric field of 10 kV/cm, 800 V must be applied which is quite high and may lead to electrode deterioration after just a few sets of experiments at this voltage. Therefore, we tested the effect of 16 pulses and the results demonstrated the saturation of permeability at 1.8 kV/cm—a substantially lower electric field (Fig. 4a). To achieve the same permeability in continuous flow, 64 pulses per cell were required (Fig. 4b). Based on the ratio of pulses to be applied in stop and continuous flow, MATLAB calculations estimated the affected cell surface in continuous flow mode is approximately 16%.

These data proved that the cells undergo membrane permeabilization during PEF treatment in the microchip with a very gentle impact on cell viability. The high viability during the electroporation is attributed to the lower voltage, shorter pulse duration, and better heat dissipation in the microfluidic device³⁶. We suggested the model on how cells are affected by electric fields in stop flow and continuous flow electroporation.

We propose that the cells exhibit semi-stationary behaviour in stop flow mode, while they undergo random rotation in continuous flow. Our model did not consider the fluid turbulence resulting from bubbles on the electrodes during PEF, which may have affected cell rotation in both continuous flow and stop flow modes^{37,38}. Cell rotation can offer advantages as it evenly disperses the increase in permeability throughout the entire cell surface³⁹.

The performance of integrated sensors was investigated by applying an electric field. We monitored the oxygen concentration changes immediately after PEF treatment (Fig. 7a). A slight oxygen concentration change was captured with and without PEF treatment in cell suspension. This proves that precise oxygen monitoring can be performed in the described microfluidic system.

To observe the pH changes after PEF treatment, pH was evaluated with 1.8 kV/cm and 2.4 kV/cm electric fields and compared to the non-electroporated samples. Both samples revealed the shift from pH 7.2 to pH 8.3 with PEF treatment. A shift of one pH unit towards the alkalinity was lower than other authors demonstrated^{34,40}. This can be explained by the fact that the buffers used in the experiments differ in other publications: (1) we use two buffering agents, bicarbonate and HEPES, which accelerate the drastic pH shift; (2) the change was measured not instantaneously but rather in a few minutes after PEF treatment; and (3) we do not measure the change that has occurred at the surface of the electrode itself, where the localized change should be the strongest³⁴. With these results, we showed that our device is capable of monitoring pH in the MPS device.

Lastly, the ability to measure TEER was demonstrated using the same incorporated electrode for PEF treatment. This demonstrated the difference in the TEER parameter between samples with and without cells. It is important to note that TEER measurements are typically performed in the presence of a functional barrier, and disruptions in the barrier can be observed. However, in our case, we work with suspension cells, which do not adhere and form a confluent layer. Despite this, our inference from the TEER measurement results is that our microfluidic device is suitable for performing such measurements. This is supported by the fact that the buffer without cells exhibited lower impedance compared to the cell suspension.

To sum up, the viability and permeability results after PEF treatment confirmed the suitability of the microchip for PEF treatment of mammalian cells. Since OSTE and CoC, both materials that confine the microchannel, preserve a characteristic of non-permeability to gas, the required gases (O₂ and CO₂) should be supplied from the outside. The integrated features of monitoring oxygen and pH would enable better regulation of the cellular environment. It should also be noted that the reported results were obtained by electroporation in the buffer except for the pH measurement, however, the growth medium must be used for cell growth. Therefore, for the selection of PEF conditions for adherent cells, electroporation experiments should be performed with the cells in culture media.

Conclusions

MPS involves co-cultures in microfluidic channels, which increases their biological complexity, but poses challenges for monitoring the physiological parameters. Our developed microfluidic chip utilises OSTE as a castable material and includes integrated oxygen sensors, a pH measuring device, and TEER measurement capability. It can effectively maintain cell viability even when subjected to intense pulsed electric fields. Notably, applying PEF treatment at 1.8 kV/cm with 16 pulses in stop flow and 64 pulses per cell in continuous flow resulted in maximum permeability. Furthermore, we could accurately monitor oxygen concentration and pH changes after PEF treatment. This innovative study highlights the seamless incorporation of the PEF treatment module into an MPS device, offering a flexible and affordable solution for future developments achieved via soft lithography-based fabrication techniques. In the subsequent stages, we expect that the new MPS can be employed to culture adherent cells on the PC membrane and evaluate modifications in cellular signalling subsequent to PEF exposure.

Material and methods

Fabrication of a microfluidic chip

To produce the microchip, a pseudo-positive 3D master mold was printed from Zortrax white resin (Zortrax Ikspire, Olsztyn, Poland). To prepare the PDMS, a Sylgard 184 silicone elastomer kit (Dow Corning, USA) was used by mixing the crosslinker and the substrate in a 1:10 (w/w) ratio. The PDMS was degassed in a vacuum chamber and cast into a 3D master mold. The mold was pre-coated with a thin layer of organic mold-releasing wax. To ensure that the height of the PDMS mold was dimensionally correct, the PDMS was cast by pressing the base mold against the glass surfaces and cured at 60 °C overnight. The cast PDMS mold was removed from the 3D-printed master mold and the inlets were punched with a biopsy punch.

CoC (microscopy slide format Microfluidic Microchip Shop, Jena, Germany), was used as a base for microchip. Two CoC slides were pre-washed with acetone and rinsed with isopropanol using an ultrasonic cleaning bath for 10 min, and treated with an oxygen plasma etcher (Diener electronic, Zepto B, Germany) for 30 s at 70% power and 0.35 mbar pressure. A thin layer of gold with a chrome sublayer for adhesion was deposited through a mechanical mask by thermal evaporation on CoC slides.

The bottom CoC slide with electrodes was placed in a PDMS mold and attached to a custom 3D-printed holder. Two PTFE tubes were connected to the injection ports on the PDMS mold for injection of OSTE (Ostermer322 resin, Mercene Labs, Stockholm, Sweden). OSTE was prepared according to the instructions (1.09:1 PartA:PartB, w/w), degassed, and filled into the cavities of the CoC/PDMS construct. Initial curing of OSTE was carried out by illumination with 365 nm UV light (intensity approx. 2.04 mW/cm²) for 1 min. The device was disassembled and a porous PC membrane (ipPORE, 3 μm or 0.4 μm, Louvain-la-Neuve Belgium), pre-treated with oxygen plasma, was pressed onto the cured but still sticky OSTE layer. The bottom slide of the microchip was cured at 60 °C for 2 h. The UV-cured upper slide of the chip was then prepared likewise. Two SP-PSt6-YAU point oxygen sensors (PreSens Precision Sensing GmbH, Regensburg, Germany) were glued to the respective channel locations using Sil-Poxy™ silicone adhesive (Smooth-on Inc., PA, USA). The upper CoC/OSTE/O₂ sensor slide was pressed onto the lower CoC/OSTE/PC slide and cured at 60 °C for 2 h.

The channel height of the fabricated microchip was measured by a Vernier calliper. Mini Luer ports (Microfluidic ChipShop, Germany) were mounted with MD® medical adhesive 1403-M (Dymax, Wiesbaden, Germany) and cured for 1 min under 405 nm UV light (intensity approx. 1.95 mW/cm²). The performance of the individual electrodes was confirmed by measuring the impedance with a precision LCR-6000 m (Gwinstek, USA).

Microfluidic setup

neMESYS low-pressure syringe pump (Cetoni, Korbussen, Germany) was employed to maintain the flow rate within the channel, which was controlled through computer software. PTFE tubing with 0.8 mm inner diameter and silicon tubing with 1 mm inner diameters (Darwin Microfluidics, Paris, France) were used for the syringe pump and microchip connection. Before experiments, microchannels were washed with 70% ethanol, then with sterile deionized water, and subsequently with an electroporation buffer or RPMI-1640 medium (Corning, VA, USA). The flow rate was set to 1 μl/s for cell injection and 5 μl/s for cell collection and channel washing.

Cell line handling

Rat glioma cell line C6 (ATCC CCL-107™) was grown in RPMI-1640 medium supplemented with 10% fetal bovine serum (Gibco, Thermo Fisher Scientific, NY, USA) and antibiotics penicillin 100 U/ml and streptomycin 100 μg/ml (Gibco) at 37 °C, 5% CO₂ atmosphere in a humidified chamber. Cells were passed twice a week. For the electroporation experiments, the cells were detached by trypsinization (trypsin 0.025% and EDTA 0.02% solution) (Gibco), centrifuged, and resuspended in an electroporation buffer (0.7 mM NaCl, 1 mM KCl, 10 mM HEPES, 3 mM NaOH, 250 mM saccharose, pH 7.4)⁴¹ at a concentration of 5–10 × 10⁶ cells/ml or in RPMI-1640 supplemented with HEPES for pH measurement experiments.

PEF treatment experiments

PEF was applied using the high-power square wave pulse electroporator Elpora (Centre for Physical Sciences and Technology, Vilnius, Lithuania)⁴². The voltage of PEF treatment was determined using an oscilloscope (TDS 1012B, Tektronix, USA).

Stop flow PEF

Cells were injected into the area of electrodes at the flow rate of 1 μl/s, allowed to settle down for one minute, and subjected to 0–10 kV/cm pulsed electric field. A sequence of 8 or 16 rectangular pulses of 100 μs length and repetition frequency 1 Hz was used for pulsation, followed by incubation for 1 min. Next, the cells were moved along the microchannel by the volume between one electrode pair and the PEF treatment was repeated. To ensure that all cells received PEF treatment, the whole process was repeated twice based on the initial volume of the injected cells. The volume between one electrode pair is calculated using the following formula:

$$V_o[\mu\text{l}] = l \times w \times h, \quad (1)$$

where V_o is the volume between parallel electrodes, l is the electrode length, w is the electrode width and h is the microchannel height.

Continuous flow PEF

Cells were injected and remained in continuous flow while receiving 8 to 128 rectangular pulses of 100 μs duration at 1 Hz repetition rate. To obtain a specific number of pulses in continuous flow mode, the flow rate is calculated using the following formula:

$$v \left[\frac{\mu\text{l}}{\text{s}} \right] = \frac{4 \times V_o[\mu\text{l}] \times f[\text{Hz}]}{n[\text{pulse number}]}, \quad (2)$$

where v is the flow rate, 4 is the number of electrodes, f is the repetition rate and n is the pulse number.

For the viability studies, cells were collected after PEF treatment, seeded into a 24-well plate, and incubated for 16 h at 37 °C, 5% CO₂ atmosphere in a humidified chamber. The number of viable cells was determined with a trypan blue exclusion assay (Gibco).

For the permeability studies, cells were suspended with DAPI (ThermoFisher Scientific, IL, USA) to a $1\ \mu\text{M}$ concentration, followed by incubation for 20 min prior to the PEF treatment. After incubation, cells were injected into the microchip and PEF treatment was performed. In continuous flow experiments, cells were incubated without flow for 5 min after PEF treatment. The fluorescence emission at 455 nm of the cell suspension was measured for the excitation of 395 nm with a fluorescent spectrophotometer (LS50B, Perkin Elmer, USA).

Oxygen sensing setup

The oxygen measurement system Oxy-4 SMA (G3) meter (PreSens Precision Sensing GmbH) is connected to the support jig with polymer optical fiber (POF). POF transfers excitation light to the sensor embedded inside the microchip and the sensor responds to the meter. The PreSens Measurement Studio 2 software is used to analyse the results. The calibration of oxygen microsensors was performed using a conventional two-point calibration in oxygen-free water with 80 mM sodium sulphite, 0.25 mM cobalt nitrate as calibration point 0 and air-saturated water as calibration point 21.

Oxygen measurement experiments

The change in oxygen content between the two built-in sensors was measured in the stop flow electroporation experiments. The oxygen content was measured before and immediately after PEF treatment with various electric fields and 16 pulses. The oxygen content was measured with both sensors simultaneously and the results are presented as the difference in oxygen concentration $\Delta\%$ after (sensor 2) and before (sensor 1) PEF treatment.

pH measurement setup

The developed pH sensor module consists of photodiode optical glass filter FGL515, 515 nm long-pass (Thorlabs, USA) and white LED LEDWE-15 with forward current 25 mA, power 13.0 mW (0.013 W) (Thorlabs, USA)⁴³. The RealTerm software was used to register the results employing building 10 bit analog to digital converter. To achieve quality measurement an operational amplifier (opamp) based current to voltage converter with floating reference is employed. The second stage amplifier is introduced to increase the magnitude of an offset signal (opamp-based noninverting amplifier with variable gain) (Fig. 8). Floating reference allows extracting essential measurement data without supplementary DC components.

pH sensor consists of white LED D1 and photodiode S1, current produced by photodiode depends on pH measurements. Opamp OP1 based current to voltage converter is employed in order to produce voltage signal of desired amplitude range. Floating reference is connected to the circuit employing opamp OP3 buffer for impedance alignment. Reference is adjusted according to environmental ambient exposure during. The second stage opamp OP2 based amplifier is dedicated extract essential measurement discarding ambient exposure.

The pH calibration was performed with an RPMI medium containing both sodium bicarbonate and HEPES with four pH values ranging from 6.0 to 8.0. The pH of the cell suspension was measured during the stop flow electroporation experiments at 0, 1.8 and 2.4 kV/cm electric fields with 16 pulses. The pH is calculated using the calibration curve (Supplementary S3).

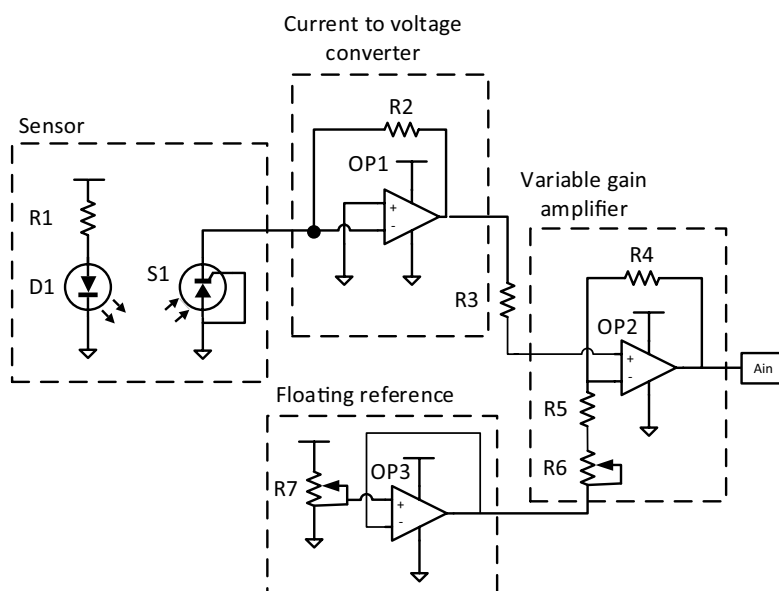


Figure 8. Circuit diagram of pH measurement consists of sensor LED D1 with current limiting resistor R1, and photodiode S1, current to voltage converter (opamp OP1 and feedback resistor R2), floating reference (potentiometer R7 and opamp OP3 as a buffer), variable gain amplifier (noninverting opamp OP2, feedback resistor R4, gain resistors R5, R6 and input resistor R3), treated reading is passed to an analog input Ain.

TEER measurement

LCR-6000m was connected to two adjacent electrodes in one plane and was used for TEER measurement in the stop flow electroporation experiments.

Data availability

The datasets generated and/or analyzed during the current study are available from the corresponding author upon reasonable request.

Received: 22 February 2024; Accepted: 6 August 2024

Published online: 12 August 2024

References

1. Tsong, T. Y. Electroporation of cell membranes. *Biophys. J.* **60**, 297–306 (1991).
2. Neumann, E., Schaefer-Ridder, M., Wang, Y. & Hofschneider, P. H. Gene transfer into mouse lyoma cells by electroporation in high electric fields. *EMBO J.* **1**, 841–845 (1982).
3. Rubinsky, B. Irreversible electroporation in medicine. *Technol. Cancer Res. Treat* **6**, 255–260 (2007).
4. Taha, A. *et al.* Pulsed electric field-assisted glycation of bovine serum albumin/starch conjugates improved their emulsifying properties. *Innovative Food Sci. Emerg. Technol.* **82**, 103190 (2022).
5. Modena, M. M., Chawla, K., Misun, P. M. & Hierlemann, A. Smart cell culture systems: Integration of sensors and actuators into microphysiological systems. *ACS Chem. Biol.* **13**, 1767–1784 (2018).
6. Wikswo, J. P. *et al.* Scaling and systems biology for integrating multiple organs-on-a-chip. *Lab. Chip* **13**, 3496–3511 (2013).
7. Bavli, D. *et al.* Real-time monitoring of metabolic function in liver-on-chip microdevices tracks the dynamics of mitochondrial dysfunction. *Proc. Natl. Acad. Sci.* **113**, E2231–E2240 (2016).
8. Eklund, S. E. *et al.* Multianalyte microphysiometry as a tool in metabolomics and systems biology. *J. Electroanal. Chem.* **587**, 333–339 (2006).
9. Cho, S., Islas-Robles, A., Nicolini, A. M., Monks, T. J. & Yoon, J.-Y. In situ, dual-mode monitoring of organ-on-a-chip with smartphone-based fluorescence microscope. *Biosensors Bioelectron.* **86**, 697–705 (2016).
10. Ferrari, E., Palma, C., Vesentini, S., Occhetta, P. & Rasponi, M. Integrating biosensors in organs-on-chip devices: A perspective on current strategies to monitor microphysiological systems. *Biosensors* **10**, 110 (2020).
11. Lucchetti, M. *et al.* Integration of multiple flexible electrodes for real-time detection of barrier formation with spatial resolution in a gut-on-chip system. *Microsyst. Nanoeng.* **10**, 1–10 (2024).
12. Bonakdar, M., Graybill, P. & Davalos, R. A microfluidic model of the blood–brain barrier to study permeabilization by pulsed electric fields. *RSC Adv.* **7**, 42811–42818 (2017).
13. Sharabi, S. *et al.* Transient blood–brain barrier disruption is induced by low pulsed electrical fields in vitro: An analysis of permeability and trans-endothelial electric resistivity. *Drug Deliv.* **26**, 459–469 (2019).
14. Chen, T. *et al.* A microphysiological system for studying barrier health of live tissues in real time. <https://doi.org/10.21203/rs.3.rs-4078220/v1> (2024).
15. Kavaliauskaitė, J., Kazlauskaitė, A., Lazutka, J. R., Mozolevskis, G. & Stirkė, A. Pulsed electric fields alter expression of NF-κB promoter-controlled gene. *Int. J. Mol. Sci.* **23**, 451 (2021).
16. McKenzie, J. R., Cognata, A. C., Davis, A. N., Wikswo, J. P. & Cliffel, D. E. Real-time monitoring of cellular bioenergetics with a multianalyte screen-printed electrode. *Anal. Chem.* **87**, 7857–7864 (2015).
17. Mohd Asri, M. A., Nordin, A. N. & Ramli, N. Low-cost and cleanroom-free prototyping of microfluidic and electrochemical biosensors: Techniques in fabrication and bioconjugation. *Biomicrofluidics* **15**, 061502 (2021).
18. Auner, A. W., Tasneem, K. M., Markov, D. A., McCawley, L. J. & Hutson, M. S. Chemical-PDMS binding kinetics and implications for bioavailability in microfluidic devices. *Lab. Chip* **19**, 864–874 (2019).
19. Rahimnejad, M. *et al.* Engineered biomimetic membranes for organ-on-a-chip. *ACS Biomater. Sci. Eng.* **8**, 5038–5059 (2022).
20. Raj, M. K. & Chakraborty, S. PDMS microfluidics: A mini review. *J. Appl. Polym. Sci.* **137**, 48958 (2020).
21. Regehr, K. *et al.* Biological implications of polydimethylsiloxane-based microfluidic cell culture. *Lab. Chip* **9**, 2132–2139 (2009).
22. Y. Wang, H. Sun, W. Li, C. Hu & K. Ren. Recent progresses in microfabricating perfluorinated polymers (Teflons) and the associated new applications in microfluidics. *Microphysiol. Syst.* **2**, (2018).
23. Jia, F., Gao, Y. & Wang, H. Recent advances in drug delivery system fabricated by microfluidics for disease therapy. *Bioengineering (Basel)* **9**, 625 (2022).
24. Toepke, M. W. & Beebe, D. J. PDMS absorption of small molecules and consequences in microfluidic applications. *Lab. Chip* **6**, 1484–1486 (2006).
25. Su, X. *et al.* Microfluidic cell culture and its application in high-throughput drug screening: Cardiotoxicity assay for hERG channels. *J. Biomol. Screen* **16**, 101–111 (2011).
26. Gomez-Sjoberg, R., Leyrat, A. A., Houseman, B. T., Shokat, K. & Quake, S. R. Biocompatibility and reduced drug absorption of sol–gel-treated poly(dimethyl siloxane) for microfluidic cell culture applications. *Anal. Chem.* **82**, 8954–8960 (2010).
27. Sasaki, H., Onoe, H., Osaki, T., Kawano, R. & Takeuchi, S. Parylene-coating in PDMS microfluidic channels prevents the absorption of fluorescent dyes. *Sensors Actuators B Chem.* **150**, 478–482 (2010).
28. Carlborg, C. F., Haraldsson, T., Öberg, K., Malkoch, M. & Wijngaart, W. Beyond PDMS: Off-stoichiometry thiolene (OSTE) based soft lithography for rapid prototyping of microfluidic devices. *Lab. Chip* **11**, 3136–3147 (2011).
29. Teng, H. Overview of the development of the fluoropolymer industry. *Appl. Sci.* **2**, 496–512 (2012).
30. Rimsa, R. *et al.* Lung on a chip development from off-stoichiometry thiol-ene polymer. *Micromachines (Basel)* **12**, 546 (2021).
31. Priedols, M. *et al.* Bifurcated asymmetric field flow fractionation of nanoparticles in PDMS-free microfluidic devices for applications in label-free extracellular vesicle separation. *Polymers* **15**, 789 (2023).
32. Fox, M. B. *et al.* Electroporation of cells in microfluidic devices: A review. *Anal. Bioanal. Chem.* **385**, 474–485 (2006).
33. Le Gac, S. & van Uiter, I. Electroporation in microfluidic devices. in *Handbook of Electroporation* (ed. Miklavcic, D.) 1–20 (Springer International Publishing, 2016). https://doi.org/10.1007/978-3-319-26779-1_136-1.
34. Li, Y. *et al.* Electroporation on microchips: The harmful effects of pH changes and scaling down. *Sci. Rep.* **5**, 17817 (2015).
35. Turjanski, P. *et al.* The role of pH fronts in reversible electroporation. *PLOS ONE* **6**, e17303 (2011).
36. Garcia, P. A., Ge, Z., Moran, J. L. & Buie, C. R. Microfluidic screening of electric fields for electroporation. *Sci. Rep.* **6**, 21238 (2016).
37. Jiao, Y., Wang, L. & Chen, J. A mesoscale bubble-induced turbulence model and simulation of gas–liquid flows. *Phys. Fluids* **35**, 013314 (2023).
38. Rodriguez Osuna, I. A., Cobelli, P. & Olai, N. Bubble formation in pulsed electric field technology may pose limitations. *Micromachines (Basel)* **13**, 1234 (2022).
39. Wang, J., Zhan, Y., Ugaz, V. M. & Lu, C. Vortex-assisted DNA delivery. *Lab. Chip* **10**, 2057–2061 (2010).

40. Gryś, M., Madeja, Z. & Korohoda, W. Avoiding the side effects of electric current pulse application to electroporated cells in disposable small volume cuvettes assures good cell survival. *Cell. Mol. Biol. Lett.* **22**, 1 (2017).
41. Sherba, J. J. *et al.* The effects of electroporation buffer composition on cell viability and electro-transfection efficiency. *Sci. Rep.* **10**, 3053 (2020).
42. Stankevič, V. *et al.* Compact square-wave pulse electroporator with controlled electroporation efficiency and cell viability. *Symmetry* **12**, 412 (2020).
43. Mousavi Shaegh, S. A. *et al.* A microfluidic optical platform for real-time monitoring of pH and oxygen in microfluidic bioreactors and organ-on-chip devices. *Biomicrofluidics* **10**, 044111 (2016).

Acknowledgements

A.S. acknowledges to the ERDF PostDoc project No. 1.1.1.2/VIAA/4/20/739. We acknowledge Vilius Vertelis for electrode deposition, Skirmantas Kersulis for expertise in PEF, and Agne Damarackaite for her assistance in performing the experiments.

Author contributions

N.B – developed the device, designed, performed experiments and analyzed data, wrote the manuscript and prepared the figures. E.A. – performed 3D printing, E.A. and K.K. fabricated the microfluidic device. J.D. performed simulations and visualization of the manuscript. M.S. developed a software and hardware for pH registration. G.M provided the conceptualisation and funding. A.S conceived, initiated, and supervised the overall project, reviewed and edited the manuscript.

Competing interests

The authors declare no competing interests.

Additional information

Supplementary Information The online version contains supplementary material available at <https://doi.org/10.1038/s41598-024-69693-w>.

Correspondence and requests for materials should be addressed to N.B. or A.S.

Reprints and permissions information is available at www.nature.com/reprints.

Publisher's note Springer Nature remains neutral with regard to jurisdictional claims in published maps and institutional affiliations.

Open Access This article is licensed under a Creative Commons Attribution-NonCommercial-NoDerivatives 4.0 International License, which permits any non-commercial use, sharing, distribution and reproduction in any medium or format, as long as you give appropriate credit to the original author(s) and the source, provide a link to the Creative Commons licence, and indicate if you modified the licensed material. You do not have permission under this licence to share adapted material derived from this article or parts of it. The images or other third party material in this article are included in the article's Creative Commons licence, unless indicated otherwise in a credit line to the material. If material is not included in the article's Creative Commons licence and your intended use is not permitted by statutory regulation or exceeds the permitted use, you will need to obtain permission directly from the copyright holder. To view a copy of this licence, visit <http://creativecommons.org/licenses/by-nc-nd/4.0/>.

© The Author(s) 2024